Quasielastic ^{3}He$(e, e'p)^2$H Reaction at $Q^2 = 1.5$ GeV^2 for Recoil Momenta up to 1 GeV/c

M. M. Rvachev,[1] F. Benmokhtar,[2,3] E. Penel-Nottaris,[4] K. A. Aniol,[5] W. Bertozzi,[1] W. U. Boeglin,[6] F. Butaru,[4] J. R. Calarco,[7] Z. Chai,[1] C. C. Chang,[8] J.-P. Chen,[9] E. Chudakov,[9] E. Cisbani,[10] A. Cochran,[11] J. Cornejo,[5] S. Dieterich,[2] P. Djawotho,[12] W. Duran,[5] M. B. Epstein,[5] J. M. Finn,[12] K. G. Fissum,[13] A. Frahi-Amroun,[3] S. Frullani,[10] C. Furget,[4] F. Garibaldi,[10] O. Gayou,[12] S. Gilad,[1] R. Gilman,[2,9] C. Glashausser,[2] J.-O. Hansen,[9] D. W. Higinbotham,[1,9] A. Hotta,[14] B. Hu,[11] M. Iodice,[10] R. Iomni,[10] C. W. de Jager,[9] X. Jiang,[2] M. K. Jones,[8,9] J. J. Kelly,[8] S. Kox,[4] M. Kuss,[9] J. M. Laget,[15] R. De Leo,[16] J. J. LeRose,[9] E. Liatard,[4] R. Lindgren,[17] N. Liyanage,[9] R. W. Lourie,[18] S. Malov,[2] D. J. Margaziotis,[5] P. Markowitz,[6] F. Merchez,[4] R. Michaels,[9] J. Mitchell,[9] J. Mougey,[4] C. F. Perdrisat,[12] V. A. Punjabi,[19] G. Quéméner,[4] R. D. Ransome,[2] J.-S. Réal,[4] R. Roché,[20] F. Sabatié,[21] A. Saha,[9] D. Simon,[21] S. Strauch,[2] R. Suleiman,[1] T. Tamae,[22] J. A. Templon,[23] R. Tieulent,[4] H. Ueno,[24] P. E. Ulmer,[21] G. M. Urciuoli,[10] E. Voutier,[4] K. Wijesooriya,[25] and B. Wojtsekhowski[9]

(Jefferson Lab Hall A Collaboration)

[1]*Massachusetts Institute of Technology, Cambridge, Massachusetts 02139, USA*
[2]*Rutgers, The State University of New Jersey, Piscataway, New Jersey 08854, USA*
[3]*Université des Sciences et de la Technologie, BP 32, El Alia, Bab Ezzouar, 16111 Alger, Algeria*
[4]*Laboratoire de Physique Subatomique et de Cosmologie, F-38026 Grenoble, France*
[5]*California State University Los Angeles, Los Angeles, California 90032, USA*
[6]*Florida International University, Miami, Florida 33199, USA*
[7]*University of New Hampshire, Durham, New Hampshire 03824, USA*
[8]*University of Maryland, College Park, Maryland 20742, USA*
[9]*Thomas Jefferson National Accelerator Facility, Newport News, Virginia 23606, USA*
[10]*INFN, Sezione Sanitá and Istituto Superiore di Sanitá, Laboratorio di Fisica, I-00161 Rome, Italy*
[11]*Hampton University, Hampton, Virginia 23668, USA*
[12]*College of William and Mary, Williamsburg, Virginia 23187, USA*
[13]*University of Lund, Box 118, SE-221 00 Lund, Sweden*
[14]*University of Massachusetts, Amherst, Massachusetts 01003, USA*
[15]*CEA-Saclay, F-91191 Gif Sur-Yvette CEDEX, France*
[16]*INFN, Sezione di Bari and University of Bari, I-70126 Bari, Italy*
[17]*University of Virginia, Charlottesville, Virginia 22901, USA*
[18]*State University of New York at Stony Brook, Stony Brook, New York 11794, USA*
[19]*Norfolk State University, Norfolk, Virginia 23504, USA*
[20]*Florida State University, Tallahassee, Florida 32306, USA*
[21]*Old Dominion University, Norfolk, Virginia 23529, USA*
[22]*Tohoku University, Sendai 980, Japan*
[23]*University of Georgia, Athens, Georgia 30602, USA*
[24]*Yamagata University, Kojirakawa-machi 1-4-12, Yamagata 990-8560, Japan*
[25]*University of Illinois at Urbana Champaign, Urbana, Illinois 61801, USA*

(Received 10 September 2004; published 20 May 2005)

We have studied the quasielastic ^{3}He$(e, e'p)^2$H reaction in perpendicular coplanar kinematics, with the energy and the momentum transferred by the electron fixed at 840 MeV and 1502 MeV/c, respectively. The ^{3}He$(e, e'p)^2$H cross section was measured for missing momenta up to 1000 MeV/c, while the A_{TL} asymmetry was extracted for missing momenta up to 660 MeV/c. For missing momenta up to 150 MeV/c, the cross section is described by variational calculations using modern ^{3}He wave functions. For missing momenta from 150 to 750 MeV/c, strong final-state interaction effects are observed. Near 1000 MeV/c, the experimental cross section is more than an order of magnitude larger than predicted by available theories. The A_{TL} asymmetry displays characteristic features of broken factorization with a structure that is similar to that generated by available models.

DOI: 10.1103/PhysRevLett.94.192302 PACS numbers: 21.45.+v, 25.30.Dh, 27.10.+h

Microscopic calculations make it now possible to calculate the bound-state and scattering-state wave functions from Hamiltonian models for processes involving three-nucleon systems [1]. Thus, using modern (nonrelativistic) Faddeev [2,3] and variational [4] techniques to solve the three-body problem, one hopes to test the ability to predict the structure of three-body systems with state-of-the-art realistic NN potentials. However, reaction-dynamics pro-

cesses such as final-state interactions (FSI), two-body currents (meson exchange and isobar), as well as relativity have to be taken into account in the data interpretation. Unfortunately, the above mentioned techniques are not sufficiently developed to reliably describe the reaction dynamics at high energies. As such, they would benefit tremendously from data for guidance in their development process.

High-energy electron beams with high currents and 100% duty factor at the Thomas Jefferson National Accelerator Facility (JLab) enable experiments to reach new kinematic domains and levels of precision in utilizing the $(e, e'p)$ reaction to study nuclear structure and reaction dynamics. In this Letter, we address the interplay between nuclear structure and reaction dynamics by providing an extensive and precise data set that includes cross sections and the A_{TL} asymmetry for the ^{3}He$(e, e'p)^2$H reaction in constant quasielastic electron kinematics. This data set significantly extends the available data in both the transferred four-momentum and the recoil momentum of the undetected deuteron (missing momentum), p_m.

Measurements were performed using an incident beam of 4806 MeV and the two high-resolution spectrometer system (HRS) in Hall A of JLab. A detailed description of the Hall A instrumentation is available in [5]. Electrons (protons) were detected with the left (right) HRS, respectively, HRS-L and HRS-R. Scattered electrons were detected at a central scattering angle of 16.4° and a central momentum of 3966 MeV/c, corresponding to the quasielastic knockout of protons from the ^{3}He nucleus with transferred three-momentum $|\vec{q}| = 1502$ MeV/c, energy $\omega = 840$ MeV, four-momentum $Q^2 = 1.55$ GeV^2, and Bjorken scaling variable $x_B = Q^2/(2\omega M_p) = 0.98$. The range in accepted Q^2 and ω was ± 0.12 GeV^2 and ± 20 MeV, respectively. The ejected proton was detected in coincidence with the scattered electron in coplanar kinematics over a range of angles and momenta (see Table I), to measure the p_m dependence of the ^{3}He$(e, e'p)^2$H cross section on both sides of the momentum-transfer direction.

A cooled, 10.3 cm diameter ^{3}He gas target was used at temperature $T = 6.3$ K and pressures $P = 8.30$–10.9 atm, corresponding to densities $\rho = 0.0603$–0.0724 g/cm^3. Relative changes in the target density were monitored by observing changes in the rate of singles events in the fixed HRS-L per unit beam charge passing through the target. The target density was determined by measuring the elastic ^{3}He(e, e) cross section at a beam energy of 644 MeV ($\theta_e = 30.7°$, $Q^2 = 0.11$ GeV^2), and normalizing it to the cross section derived from a fit to the world data of ^{3}He elastic form factors [6]. The overall normalization uncertainty of the ^{3}He density is estimated to be 2.9%, obtained as the quadratic sum of the systematic uncertainty of our ^{3}He elastic cross-section measurement (2.4%), the statistical uncertainty (0.5%), the uncertainty in the ^{3}He form factors (1.5%), and a 0.5% uncertainty due to possible fluctuations in the target density during the change of the beam energy from 4806 to 644 MeV.

TABLE I. Central kinematic values of the ^{3}He$(e, e'p)^2$H measurements. Listed are the central settings of the hadron (HRS-R) spectrometer (momentum P_p, angle θ_p, and missing momentum p_m). Negative (positive) p_m corresponds to the detected proton forward (backward) of $\vec{q}$. The electron kinematics were fixed, at incident and scattered electron energies of $E = 4806$ MeV and $E' = 3966$ MeV, respectively, and scattering angle of $\theta_e = 16.4°$ ($Q^2 = 1.55$ GeV^2, $|\vec{q}| = 1502$ MeV/c, $\omega = 840$ MeV, $x_B = 0.98$).

p_m MeV/c	P_p MeV/c	θ_p deg
−550	1406	26.79
−425	1444	31.84
−300	1472	36.76
−150	1493	42.56
0	1500	48.30
150	1493	54.04
300	1472	59.83
425	1444	64.76
550	1406	69.80
750	1327	78.28
1000	1171	89.95

Event triggers were formed by coincident signals from scintillator arrays. Particle tracks were reconstructed using the HRS vertical drift chambers. The small π^- background in the HRS-L was rejected using a CO_2 gas Čerenkov detector. In the HRS-R, coincident π^+, ^{2}H, and ^{3}H were separated from the protons using the time difference between particles detected in the two spectrometers. Most of the accidental coincident events were rejected by cuts on the difference between interaction points in the target along the beam as reconstructed by the two spectrometers, $|z_h - z_e| \leq 2$ cm, where the interaction-point resolution was about 8 mm (FWHM), and on the E_m (missing energy) spectrum. The E_m resolution was 2.4 MeV (FWHM). The remaining accidental background was subtracted using the coincidence timing between the spectrometers. Events originating in the target Al walls were rejected by requiring reconstructed events to originate within 3.5 cm from the target center. With these cuts, the signal-to-noise ratio in the most extreme kinematics, for $p_m \approx 1$ GeV/c, was 50/1, and, in the worse case, for $p_m \approx -650$ MeV/c, about 0.8/1 (see Fig. 1).

In the cross-section analysis, a flat acceptance region of both HRSs was defined using an R-function cut imposed on the target variables. An R function is a function whose sign is completely determined by the signs of its arguments [7,8]. Using constructive-geometrical properties of R functions, one can define a complicated multidimensional acceptance region as an analytical expression, and vary the region's boundaries until the phase space is maximized

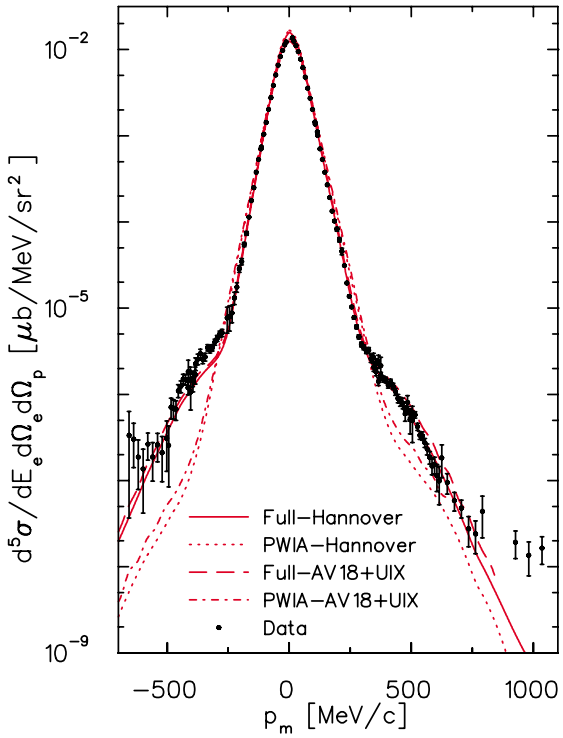

FIG. 1 (color online). Measured ^{3}He$(e, e'p)^2$H cross section as a function of the missing momentum, p_m. Also displayed are PWIA and full calculations in the diagrammatic approach for two different ground-state wave functions.

within the flat acceptance region of the spectrometers [9]. The use of R functions allowed us to double the accepted phase space compared to the commonly used rectangular cuts on target variables.

The ^{3}He$(e, e'p)^2$H cross section was extracted using the simulation program MCEEP (Monte Carlo for Electro-Nuclear Coincidence Experiments) [10], taking into account the effects of internal and external radiation, particle energy loss, deviations from monochromaticity of the beam, and spectrometer resolutions. For each p_m bin, the simulated yields were varied by modifying the spectral function used in MCEEP to achieve calculated cross sections that agreed with the measured ones in both the ^{3}He$(e, e'p)^2$H E_m bin and the adjacent ^{3}He$(e, e'p)(pn)$ E_m bin [9]. Cross sections were extracted from the reweighted ^{3}He$(e, e'p)^2$H yield, corrected for radiation, and for contributions from ^{3}He$(e, e'p)(pn)$ to each ^{3}He$(e, e'p)^2$H kinematic bin. On average, these contributions were about 3%. Within each bin, the simulated ^{3}He$(e, e'p)$ cross section was assumed to depend on the σ_{cc1} prescription of de Forest [11] for the off-shell electron-proton cross section. This technique allows one to separate the p_m dependence of the reaction from the rapid dependence on the electron kinematics [9]. In addition to the overall normalization uncertainty (2.9%, see above), the overall systematic uncertainty was 3.4% dominated by uncertainties in the solid angle (2.0%), the selection (E_m cut) of the two-body breakup reaction channel (1.5%), and the knowledge of the effective target length via a cut on the interaction vertex location (1.4%).

The extracted ^{3}He$(e, e'p)^2$H cross section is plotted in Fig. 1 as a function of p_m. We note that the range of p_m measured (resulting in measured cross-section values varying over 6 orders of magnitude) is significantly larger than in any other previous measurement. Moreover, contrary to previous experiments [12–14], our measurements over this entire range were performed at fixed electron kinematics.

Also displayed in Fig. 1 are four theoretical curves. The plane-wave impulse approximation (PWIA) and full Hannover calculations use the Hannover bound-nucleon wave function [15] corresponding to the solution to the three-body Faddeev equation with the Paris NN potential and no three-body forces. The AV18 + UIX curves are the same PWIA and full calculations, respectively, but with a bound-state nuclear wave function derived by a variational technique using the Argonne V18 NN potential and the Urbana IX three-body force [16]. All calculations use a diagrammatic approach. The kinematics as well as the nucleon and meson propagators are relativistic, and no restricted angular (Glauber-type) approximation has been made in the various loop integrals. Details of the model can be found in [17]. The PWIA curves include only one-body interactions, while the full calculations include FSI, meson (π and ρ) exchange, and intermediate Δ formation currents, as well as three-body (three-nucleon π double scattering) amplitudes. The FSI in these calculations follow a global parametrization of the NN scattering amplitude, obtained from experiments in LANL, SATURNE, and COSY [18]. On the scale of Fig. 1, the differences between the calculations using the two ground-state wave functions are very small. By far, FSI constitute the major difference between the full and PWIA calculations. Meson exchange and intermediate Δ current contributions are generally small (up to 21%–25%), and the three-body contributions are negligible [18].

Three regions of p_m can be discerned in Fig. 1. For $|\vec{p}_m|$ below $\sim$150 MeV/c, roughly within the Fermi momentum, the deuteron can be viewed as only marginally involved in the interaction [19]. Hence, the data are expected to be dominated by the single-proton characteristics of the ^{3}He wave function. As can be observed, both the PWIA and full curves describe the data quite well, and the difference between them is rather small (see also Fig. 2 for details). For $|\vec{p}_m|$ between 150 and 750 MeV/c, well above the Fermi momentum, the cross section is expected to be dominated by the dynamics of the reaction. Indeed, very large contributions from dynamical effects are observed. While the full calculations describe the data very well, the PWIA curves overpredict the data by up to a factor of 2 for $150 \leq |\vec{p}_m| \leq 300$ MeV/c and underpredict them by up to an order of magnitude for $400 \leq |\vec{p}_m| \leq 750$ MeV/c. The differences between the two PWIA and

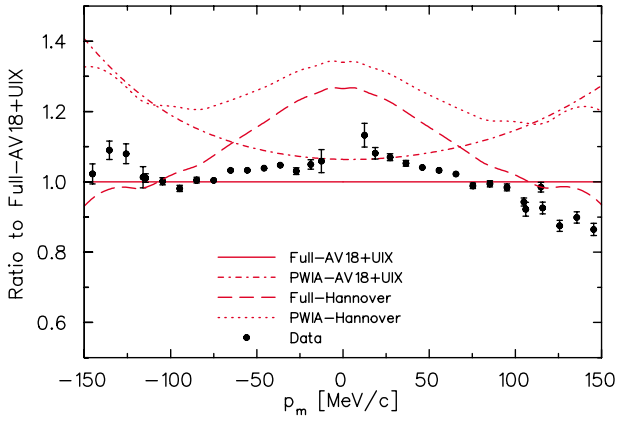

FIG. 2 (color online). Same data as in Fig. 1 for low p_m only, but shown as a ratio to the full calculation that uses the ground-state wave function generated from the AV18 *NN* potential and the Urbana IX three-nucleon force. Also shown are the ratios to this calculation of the full calculation that uses the Hannover GSWF, as well as of the two corresponding PWIA curves.

two full-calculation curves are very much dominated by FSI. At $x_B = 1$, the on-shell rescattering of the fast nucleon on a nucleon at rest is preferred and the contribution of FSI is maximal. Because the *NN* scattering amplitude is almost purely absorptive in the JLab energy range, the corresponding FSI amplitude interferes destructively with the PWIA amplitude below, and constructively above $p_m \approx 300$ MeV/c [18]. We note the difference in cross sections in this region for negative and positive p_m, and it is discussed below. For p_m larger than 750 MeV/c, the calculations gradually deviate from the experimental data: at 1000 MeV/c, they grossly underpredict the measured cross section by more than an order of magnitude. Whether it is a consequence of the truncation of the diagrammatic expansion or a signature of other degrees of freedom is an open question.

The sensitivity of the data to the details of the wave function at low $|\vec{p}_m|$ is shown in Fig. 2. In order to enhance the details, Fig. 2 displays the low $|\vec{p}_m|$ subset of the data from Fig. 1 as a ratio to the full calculation using the AV18 *NN* potential and the Urbana IX three-nucleon force. Also displayed are the ratios to the same calculation of the full Hannover and the two corresponding PWIA calculations. As already noted, in the low $|\vec{p}_m|$ region, we expect reaction effects such as FSI and two-body currents to be relatively small as compared to higher $|\vec{p}_m|$ (Fig. 1), and hence the data to be more sensitive to the details of the calculated ground-state wave functions than to the uncertainty in describing reaction dynamics. As can be seen in the figure, the curves produced by this model are mainly sensitive to the details of the bound-nucleon wave function. We note that, for p_m below 50 MeV/c, the calculations are purely coplanar perpendicular kinematics, whereas experimentally, because of the large $|\vec{q}|$, it is difficult to avoid contamination with parallel and out-of-plane components. For $|\vec{p}_m| > 50$ MeV/c, we observe that the curve that best agrees with the data is the full AV18 + UIX. We suggest that this better agreement with the data is related to the fact that the wave function generated from the AV18 + UIX potentials reproduces the correct ^{3}He binding energy (by construction), while the Hannover wave function that does not include three-body forces underbinds ^{3}He by $\sim$0.7 MeV.

The A_{TL} asymmetry was extracted for $0 \leq |\vec{p}_m| \leq 660$ MeV/c according to

$$A_{TL} = \frac{\sigma_+ - \sigma_-}{\sigma_+ + \sigma_-}, \tag{1}$$

where σ_+ and σ_- are coplanar ^{3}He$(e, e'p)^2$H cross sections measured at positive and negative missing momentum, respectively. The A_{TL} observable down plays the significance of the ground-state wave function, by virtue of the ratio involved in its definition [20], and there exist indications that it is sensitive to relativistic effects [21] and to mechanisms that break the simple factorization scheme of PWIA cross sections [22].

Figure 3 displays the extracted A_{TL} data with the PWIA and full calculations using the two ground-state wave functions described above. The difference in the two ground-state wave functions has a very small effect in the full calculations. In contrast to the PWIA calculations, the

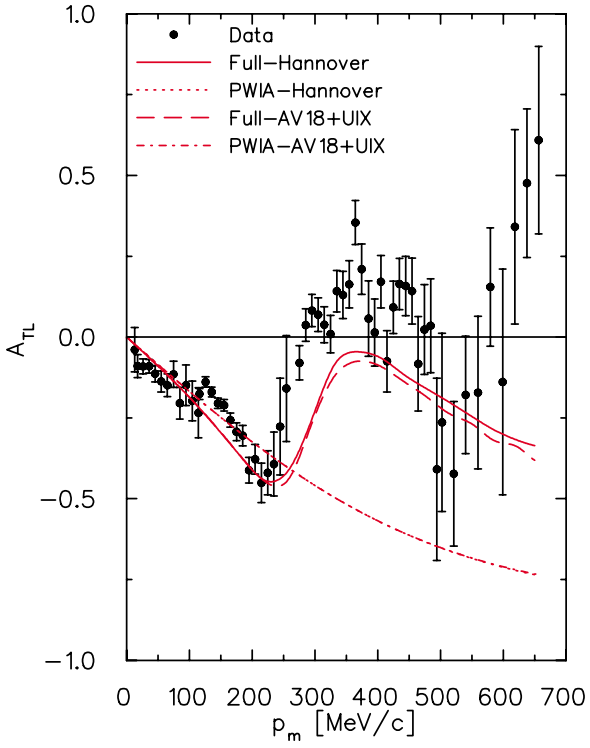

FIG. 3 (color online). The measured A_{TL} asymmetry. The curves are the same four calculations used in Figs. 1 and 2; by definition, the two PWIA curves are indistinguishable.

measured A_{TL} displays a structure characteristic of broken factorization [22]: the oscillating pattern of A_{TL} comes directly from the interference between different reaction amplitudes. Both full calculations display a structure similar to that of the data. Such structure in A_{TL} was previously observed in the quasielastic removal of p-shell protons in the $^{16}\mathrm{O}(e, e'p)$ reaction [23], and was well reproduced by the relativistic distorted-wave impulse approximation calculations by Udias *et al.* [24]. In that case, broken factorization was attributed to dynamical relativistic effects, the enhancement of the lower components of the Dirac spinors. However, these effects are less important in this experiment because of the low nuclear density of ^{3}He [25]. Rather, in this case the factorization is broken by the strong interference between the PWIA and rescattering amplitudes [18].

In summary, we measured the $^3\mathrm{He}(e, e'p)^2\mathrm{H}$ cross sections and A_{TL} asymmetry at $Q^2 = 1.55$ GeV^2 and $x_B = 0.98$. For $|\vec{p}_m|$ below 150 MeV/c, the data are mostly sensitive to the details of the bound-state wave function. The best agreement is observed with calculations using a ^{3}He ground-state wave function generated from the Argonne V18 NN potential and the Urbana IX three-nucleon force, which also better reproduces the ^{3}He binding energy. For $|\vec{p}_m|$ from 150 to 750 MeV/c, strong FSI effects are observed as quenching (enhancement) of the cross section below (above) $|\vec{p}_m|$ of about 300 MeV/c. For missing momenta from 750 to 1000 MeV/c, the measured $^3\mathrm{He}(e, e'p)^2\mathrm{H}$ cross sections are increasingly larger (more than an order of magnitude at 1000 MeV/c) than predicted by available theories. Whether it is a consequence of the truncation of the diagrammatic expansion or a signature of the existence of exotic effects is an open question. The measured A_{TL} displays strong structure characteristic of broken factorization due to interference between the PWIA and rescattering amplitudes. Calculations using a diagrammatic method describe well the p_m dependence of the cross section up to $|\vec{p}_m| = 750$ MeV/c. Other calculations of this reaction [25–27] that have recently become available similarly interpret the data.

This work was supported by the U.S. Department of Energy (DOE) Contract No. DE-AC05-84ER40150, Modification No. M175, under which the Southern Universities Research Association (SURA) operates the Thomas Jefferson National Accelerator Facility, the National Science Foundation, the Italian Istituto Nazionale di Fisica Nucleare (INFN), the French Atomic Energy Commission and National Center of Scientific Research, the Natural Science and Engineering Research Council of Canada, and Grant-in-Aid for Scientific Research (KAKENHI) (Grant No. 14540239) from the Japan Society for Promotion of Science (JSPS).

[1] L. E. Marcucci, M. Viviani, R. Schiavilla, A. Kievsky, and S. Rosati, Eur. Phys. J. A **24**, 95 (2005).
[2] A. Nogga, H. Kamada, and W. Glockle, Phys. Rev. Lett. **85**, 944 (2000).
[3] A. Nogga, H. Kamada, W. Glockle, and B. R. Barrett, Phys. Rev. C **65**, 054003 (2002).
[4] J. Carlson and R. Schiavilla, Rev. Mod. Phys. **70**, 743 (1998).
[5] J. Alcorn *et al.*, Nucl. Instrum. Methods Phys. Res., Sect. A **522**, 294 (2004).
[6] A. Amroun *et al.*, Nucl. Phys. **A579**, 596 (1994).
[7] V. L. Rvachev and T. I. Sheiko, Appl. Mech. Rev. **48**, 151 (1995).
[8] V. L. Rvachev, *Theory of R-functions and Some Applications* (Naukova Dumka, Kiev, Ukraine, 1982), in Russian.
[9] M. M. Rvachev, Ph.D. thesis, Massachusetts Institute of Technology, 2003, http://theses.mit.edu..
[10] P. Ulmer, computer code MCEEP v.3.4, 2000.
[11] T. de Forest, Jr., Nucl. Phys. **A392**, 232 (1983).
[12] E. Jans *et al.*, Phys. Rev. Lett. **49**, 974 (1982).
[13] C. Marchand *et al.*, Phys. Rev. Lett. **60**, 1703 (1988).
[14] R. Florizone *et al.*, Phys. Rev. Lett. **83**, 2308 (1999).
[15] R. W. Schulze and P. U. Sauer, Phys. Rev. C **48**, 38 (1993).
[16] J. Forest *et al.*, Phys. Rev. C **54**, 646 (1996).
[17] J.-M. Laget, Nucl. Phys. **A579**, 333 (1994).
[18] J.-M. Laget, Phys. Lett. B **609**, 49 (2005).
[19] E. Jans *et al.*, Nucl. Phys. **A475**, 687 (1987).
[20] J. J. Kelly, Adv. Nucl. Phys. **23**, 75 (1996).
[21] S. Gilad, W. Bertozzi, and Z. L. Zhou, Nucl. Phys. **A631**, 276c (1998).
[22] J. Udias, J. Javier, E. M. de Guerra, A. Escuderos, and J. Caballero, in Proceedings of the V Workshop on Electromagnetic Induced Two-Hadron Emission, Lund, Sweden, 2001, nucl-th/0109077.
[23] J. Gao *et al.*, Phys. Rev. Lett. **84**, 3265 (2000).
[24] J. M. Udias, J. A. Caballero, E. MoyadeGuerra, J. E. Amaro, and T. W. Donnelly, Phys. Rev. Lett. **83**, 5451 (1999).
[25] J. Udias, in Proceedings of the XXIII International Workshop on Nuclear Theory, Rila, Bulgaria, 2004, edited by S. Dimitrova (Heron Press, Sofia, Bulgaria, to be published).
[26] C. Ciofi degli Atti and L. P. Kaptari, Phys. Rev. C **71**, 024005 (2005).
[27] R. Schiavilla, O. Benhar, A. Kievsty, L. Marcucci, and M. Viviani (to be published).